

Reduction of boundary effects in the spiral MRI experiment PROMISE

J. Szklarski*

Astrophysikalisches Institut Potsdam, An der Sternwarte 16, D-14482 Potsdam, Germany

Received 2007 April 16, accepted later

Published online later

Key words methods: numerical – magnetic fields – magnetohydrodynamics (MHD)

Magnetorotational instability (MRI) is one of the most important and most common instabilities in astrophysics. It is widely accepted that it serves as a source of turbulent viscosity in accretion disks – the most energy efficient objects in the Universe. However it is very difficult to bring this process down on earth and model it in a laboratory experiment. Several different approaches have been proposed, one of the most recent is PROMISE (Potsdam-ROssendorf Magnetorotational InStability Experiment). It consists of a flow of a liquid metal between two rotating cylinders under applied current-free spiral magnetic field. The cylinders must be covered with plates which introduce additional end-effects which alter the flow and make it more difficult to clearly distinguish between MRI stable and unstable state. In this paper we propose simple and inexpensive improvement to the PROMISE experiment which would reduce those undesirable effects.

© 2007 WILEY-VCH Verlag GmbH & Co. KGaA, Weinheim

1 Introduction

Velikhov (1959) showed that, for ideal magnetohydrodynamics, an axial magnetic field applied to a flow of a liquid metal between two concentric, differentially rotating cylinders (Taylor-Couette flow) can lower the critical rotation ratio or even destabilize the flow, although it is hydrodynamically stable (when the Prandtl number is large enough). That type of instability is called magnetorotational instability, and not long ago Balbus & Hawley (1991) demonstrated that it plays an important role in astrophysics. MRI serves as an essential mechanism for transporting angular momentum in a wide range of astrophysical objects, stellar interiors, jets and in particular it is crucial for process of accretion where it provides necessary amount of turbulent viscosity. Recent experiments by Ji et al. (2006) suggested that purely hydrodynamical quasi-Keplerian flows, i.e. Taylor-Couette flows which resemble Keplerian disks, do not provide viscosity required to transport the angular momentum effectively, and therefore this instability is ruled out as a source of viscous turbulence in the disks.

One of the most convenient laboratory models for MRI is still the magnetohydrodynamical, cylindrical Taylor-Couette flow with an imposed external magnetic field along the axis (Rüdiger & Zhang 2001; Ji, Goodman & Kageyama 2001). For magnetic Prandtl numbers $P_m \approx 1-10$ the axial field (when not too strong) reduces the critical Reynolds number for instability and, more importantly, also introduces instability for flows which are always stable for non-magnetic cases (see e.g. Rüdiger, Schultz & Shalybkov 2003; Barenghi et al. 2004). The unstable state is characterized by classical Taylor vortices. Regrettably, laboratory liquid metals possess very small magnetic Prandtl numbers

(due to low conductivity) so that for a purely axial field the critical Reynolds number is of order $O(10^6)$, and therefore vast rotation rates are necessary for MRI to grow.

Recently it has been shown by Hollerbach & Rüdiger (2005) and Rüdiger et al. (2005) that a current-free external azimuthal magnetic field in addition to the axial one can reduce the critical Reynolds number to $O(10^3)$ which makes it much easier to design an MRI experiment. Moreover due to symmetry-breaking there exists a drift of Taylor vortices associated with the configuration of the applied magnetic field. The frequency of the traveling wave that can be measured and compared with theory is an important feature of this type of instability.

The idea of an additional toroidal field was successfully implemented in the PROMISE experiment by Stefani et al. (2006) where modes corresponding to so called spiral (or helical) MRI were observed for the first time (see also Rüdiger et al. 2006; Stefani et al. 2007). Results of this experiment also show that in the basic stable state, without any toroidal field, there exists a nonzero axial velocity field which arises due to presence of the rigid endplates enclosing the cylinders. These plates, undoubtedly present in any real experiment, are responsible for additional effects which do not take place for an idealized infinitely long container.

The boundary layer which exists in the vicinity of the endplates consists of an Ekman layer which is the result of the rotation of a rigid surface, and a Hartmann layer which develops when a conducting fluid is used and an external axial magnetic field is applied (see e.g. Ekman 1905; Roberts 1967). Consequently, the global properties of the flow change when compared to the idealized case of infinitely long cylinders: a secondary flow, i.e. two large Ekman vortices appear, and the Hartmann current is drawn into the bulk of the fluid. All these effects depend on the mechan-

* Corresponding author: jszklarski@aip.de

ical and magnetic properties of the lids. In the PROMISE experiment one of the lids is made of copper and is attached to the outer cylinder, the other one is a stationary plexiglass plate.

In this work we review simple improvements which can reduce undesired effects induced by the lids and provide therefore the possibility to distinguish more clearly between stable and unstable states of MRI.

2 Numerical model

We consider two concentric cylinders with radii $R_{\text{in}} = 4$ cm, $R_{\text{out}} = 8$ cm and height $H = 40$ cm which rotate with angular velocities Ω_{in} , Ω_{out} . The rotation ratio $\hat{\mu} = \Omega_{\text{out}}/\Omega_{\text{in}}$ is chosen in such a way that the flow is hydrodynamically stable, i.e. Rayleigh stability criterion $\partial_r(r^2\Omega)^2 > 0$, r being the distance from the axis of rotation, is fulfilled. Through this paper we use $\hat{\mu} = 0.27$. For infinite cylinders the basic rotational profile for the flow is the Couette solution

$$\Omega_0(r) = a + \frac{b}{r^2}, \quad (1)$$

where a , b are constants dependent on radii and rotation speeds

$$a = \Omega_{\text{in}} \frac{\hat{\mu} - \hat{\eta}^2}{1 - \hat{\eta}^2}, \quad b = \frac{1 - \hat{\mu}}{1 - \hat{\eta}^2} R_{\text{in}}^2 \Omega_{\text{in}}. \quad (2)$$

The external magnetic field (steady, current free) has the form of

$$\mathbf{B}_0 = B_0 \left(\frac{\beta R_{\text{in}}}{r} \hat{e}_\phi + \hat{e}_z \right), \quad (3)$$

and its strength is measured by the Hartmann number

$$\text{Ha} = B_0 \sqrt{\frac{R_{\text{in}}(R_{\text{out}} - R_{\text{in}})}{\mu_0 \rho \nu \eta}}. \quad (4)$$

The magnetic properties of the conducting fluid are described by the magnetic Prandtl number which is the ratio of the kinematic viscosity ν to the magnetic diffusivity η , $\text{Pm} = \nu/\eta$, μ_0 denotes the magnetic permeability, and ρ denotes the density. The Reynolds number Re is defined as $\text{Re} = \nu^{-1} \Omega_{\text{in}} \sqrt{R_{\text{in}}(R_{\text{out}} - R_{\text{in}})}$. The liquid used in the PROMISE experiment is the eutectic alloy GaInSn giving $\text{Pm} = 1.4 \times 10^{-6}$. Thus it is reasonable to solve the MHD equations (dimensionless) in the small Prandtl number limit (Youd & Barenghi 2006; Roberts 1967; Zikanov & Thess 1998),

$$\partial_t \mathbf{u} + (\mathbf{u} \cdot \nabla) \mathbf{u} = -\nabla p + \nabla^2 \mathbf{u} + \text{Ha}^2 \text{rot} \mathbf{b} \times \frac{\mathbf{B}_0}{B_0}, \quad (5)$$

$$\nabla^2 \mathbf{b} = -\text{rot}(\mathbf{u} \times \mathbf{B}_0/B_0), \quad (6)$$

and $\text{div} \mathbf{u} = 0$, $\text{div} \mathbf{b} = 0$, where \mathbf{u} is the velocity field and \mathbf{b} is the perturbed magnetic field.

We simulate the above nonlinear equations for a 2D axisymmetric flow in cylindrical coordinates (r, ϕ, z) . For details on the numerical method and the boundary conditions see Youd & Barenghi (2006) and Szklarski & Rüdiger

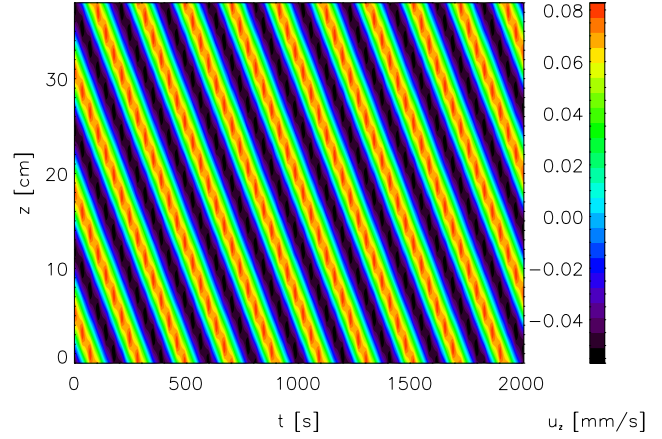


Fig. 1 Profiles of $u_z(z, t)$ at $r = R_{\text{in}} + 0.6D$ for periodic cylinders just above the critical characteristic values: $\text{Re} = 1000$, $\text{Ha} = 9.5$, $\beta = 4$. The critical Reynolds number in this case is $\text{Re}_c = 842$.

(2006). The cylinders are assumed to be perfectly conducting, and the endplates are either conducting or insulating. For the latter the pseudo-vacuum approximation is used¹.

3 Discussion of the results

From the point of view of the MRI experiment we are interested in obtaining a stable, uniform rotation profile which for subcritical characteristic parameters is as close as possible to the idealized basic state Ω_0 . On the other hand we expect a clear pattern of traveling vortices for supercritical conditions. For infinite cylinders with an external axial magnetic field and liquids with Pm of our interest the basic Couette profile Ω_0 is not altered until a critical Reynolds number of order $O(10^6-10^7)$ is reached (corresponding to a rotation frequency $f \approx 100$ Hz). For an instability due to the additional toroidal field with $\beta = 4$ we expect Re to be of order $O(10^3)$ (implying $f \approx 0.1$ Hz), Ha of order $O(10)$, and therefore we search for conditions for which the flow is closest to the Ω_0 profile for these parameters (for details on the critical values see Hollerbach & Rüdiger 2005; Rüdiger et al. 2005).

Figure 1 displays values of the velocity component u_z measured along the z axis at $r = R_{\text{in}} + 0.6D$ for supercritical values of rotation and magnetic fields. $R_{\text{in}} = 4$ cm, $R_{\text{out}} = 8$ cm, and the physical properties of gallium for the viscosity and the magnetic diffusivity are used in order to obtain values in physical scales comparable with those of the PROMISE experiment. The results in this figure are for cylinders with periodic boundary conditions so that the profiles are not constrained by end effects and are directly comparable with results from linear theory for infinite cylinders. We notice clear traces of the drifting Taylor vortices.

¹ However, even for copper the assumption for perfect conductors may be not very realistic.

3.1 Reducing endplate effects

All undesirable effects induced by the endplates arise as a consequence of vertical shears near the boundaries. Thus we attempt to reduce the shears by using appropriate boundary conditions. Some experiments (e.g. Ji et al. 2004; Noguchi et al. 2002) must deal with vast rotation rates since a toroidal field is not applied (i.e. $\beta = 0$), and the rigidly rotating boundaries dominate the whole flow (see Hollerbach & Fournier 2004). In this case it is necessary to split the endplates into many independently rotating rings (Kageyama et al. 2004; Burin et al. 2006). When the rotation rates are relatively slow, so that the corresponding Reynolds number is of order $O(10^3)$, the desired result can be achieved either by allowing the endplates to rotate rigidly and independently (see e.g. Abshagen et al. 2004) or by splitting them into two rings which are attached to both cylinders. From the technical point of view the latter configuration is easier to implement and can be considered as a possible extension to the next spiral MRI experiment.

Firstly we consider a criterion according to which we say that the boundary conditions are more suitable. In the basic state for subcritical parameters and for the case of periodic cylinders, the rotational profile of the fluid is $\Omega_0(r)$ and is independent of z , and the magnetic perturbations \mathbf{b} are zero everywhere. Introducing endplates leads to the development of z and r gradients in velocity, especially close to the vertical boundaries where $\Omega(r)$ from the bulk of the fluid must match the imposed conditions at $z = 0$, $z = H$. Consequently two Ekman vortices, new currents and magnetic fields are generated (we assume the lids to be insulating unless explicitly stated otherwise). Any deviation from Ω_0 will result in generating an azimuthal component of the magnetic field, b_ϕ , which enters the momentum equation (and in our 2D axisymmetric formulation it is the only term which gives rise to the Lorentz force). Vertical profiles of b_ϕ in the middle, i.e. for $r = D/2$, $D = R_{\text{out}} - R_{\text{in}}$, are shown in Fig. 2 for two different boundary conditions. If the endplates rotate rigidly with the outer cylinder, $\Omega_{\text{end}} = \Omega_{\text{out}}$, the Ekman circulation at the bottom lid has a clockwise direction, if they rotate with the inner cylinder, $\Omega_{\text{end}} = \Omega_{\text{in}}$, counter-clockwise – all the gradients have opposite sign. We conclude that, not surprisingly, there exists a condition with $\Omega_{\text{out}} < \Omega_{\text{endmin}} < \Omega_{\text{in}}$ for which the shears are minimized, and the generated magnetic field as well.

We are interested in obtaining a rotational profile for which the energy in b_ϕ is minimized,

$$E_b = \iint b_\phi(r, z)^2 dr dz, \quad (7)$$

where the integration is done over the total volume. As a measure of the deviation from Ω_0 one could also consider, for example, the kinetic energy of the flow, but our aim is to obtain good rotational profiles also for Ha of order 10 (and $\beta = 0$). This is not necessarily a good approach since the axial field can inhibit the flow velocity while the rotational profile will still be significantly different from Ω_0 .

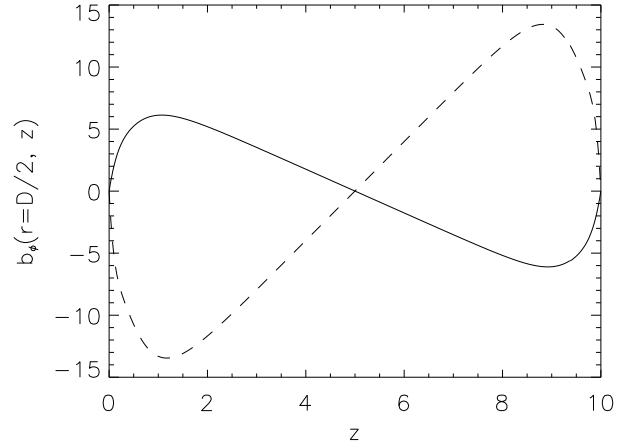


Fig. 2 Vertical profiles for induced b_ϕ in the middle of the gap, $r = D/2$ for $\beta = 0$, $\text{Re} = 100$, $\text{Ha} = 1$ and pseudo-vacuum boundary conditions. — $\Omega_{\text{end}} = \Omega_{\text{out}}$, --- $\Omega_{\text{end}} = \Omega_{\text{in}}$.

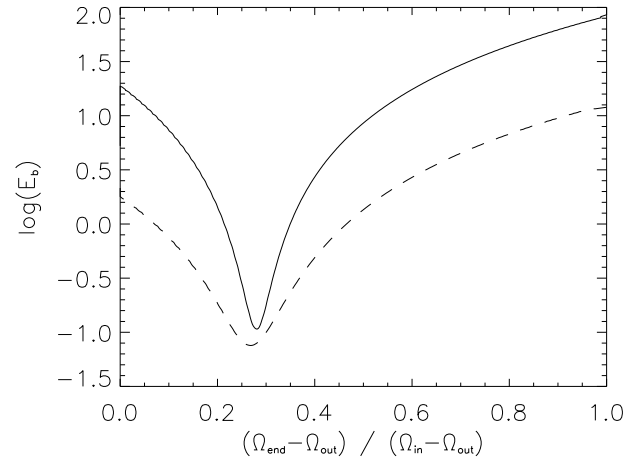


Fig. 3 The magnetic energy E_b as a function of angular velocity of independently rotating lid Ω_{end} for $\beta = 0$, $\text{Re} = 100$. — $\text{Ha} = 1$, --- $\text{Ha} = 10$.

Figure 3 shows how E_b depends on the rotation rates of the rigid endplates, $\Omega_{\text{in}} < \Omega_{\text{end}} < \Omega_{\text{out}}$. We notice that a minimum occurs for $\Omega_{\text{endmin}} \approx 0.3(\Omega_{\text{in}} - \Omega_{\text{out}}) + \Omega_{\text{out}}$ which is even three orders of magnitude smaller than for $\Omega_{\text{end}} = \Omega_{\text{in}}$.

When considering endplates divided into rings, we assume that the ring attached to the inner cylinder has a width w_1 , the other one attached to the outer cylinder has $w_2 = D - w_1$. Because it is not obvious which value for w_1 should be chosen we search for the optimal w_1 , i.e. for which E_b has a minimum, by performing simulations for several different values (Wendt 1933, for example, used $w_1/D = 0.5$). From Fig. 4 we see that the energy of the induced b_ϕ has a minimum for $w_1/D \approx 0.4$ which is roughly independent of the applied axial magnetic field. It has also been checked

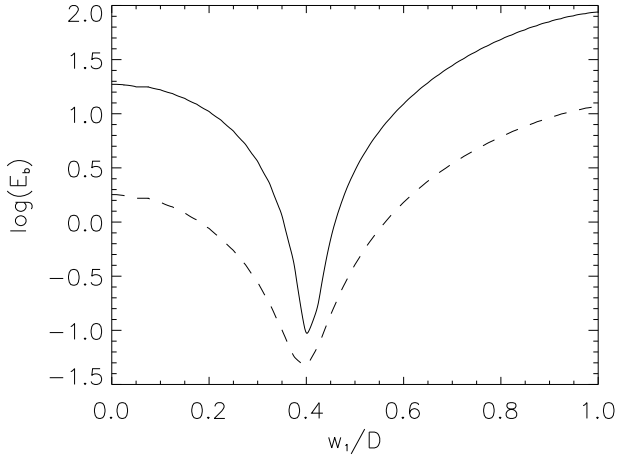


Fig. 4 The magnetic energy E_b as a function of radius of the inner ring for $\beta = 0$, $\text{Re} = 100$. — $\text{Ha} = 1$, --- $\text{Ha} = 10$.

that the minimum holds for larger Reynolds numbers (for the Fig. 3 as well). Again we notice the improvement of E_b of two to three orders of magnitude when compared to one end-ring attached either to the inner ($w_1 = D$) or outer ($w_1 = 0$) cylinder. The minimum value is very similar to that for independently rotating endplates.

A qualitative view of the resulting rotational profiles gives Fig. 5 which displays deviations of $\bar{\Omega}(r)$ – the angular velocity averaged in the z domain – from $\Omega_0(r)$ for different rotational properties of the endplates and for varied Re and magnetic fields. The case with independently rotating endplates refers to boundary conditions where both lids rotate with angular velocity Ω_{end} corresponding to the minimum value of E_b . For comparison we also present the case for two rings attached to the cylinders with equal width $w_1 = w_2 = D/2$.

We see that applying independently rotating or split endplates produce significantly more suitable profiles – flatter and closer to 1. We also notice that using $w_1 = 0.4D$ gives somewhat better results than $w_1 = 0.5D$, especially for $r > R_{\text{in}} + D/2$ where the former profile is almost flat.

3.2 Influence of the toroidal field

Figure 6 shows values of the velocity component u_z , similarly like Fig. 1 but for finite cylinders. The velocity field u_z in the basic state, i.e. $\beta = 0$ for which there is no instability, is $u_z = 0$ everywhere when considering infinite or periodic cylinders for $\text{Re} \approx 10^3$, $\text{Ha} \approx 10$. For the enclosed cylinder this is not the case. In Fig. 6a (left) we present results for symmetrically, rigidly rotating (with Ω_{out}), insulating endplates. We notice that u_z is quite large and, more importantly, time dependent (this is even more evident for u_z closer to the inner cylinder). The right panel in this figure displays the same flow with the toroidal field applied, $u_z(z)$ is averaged in time and subtracted in order to filter out the

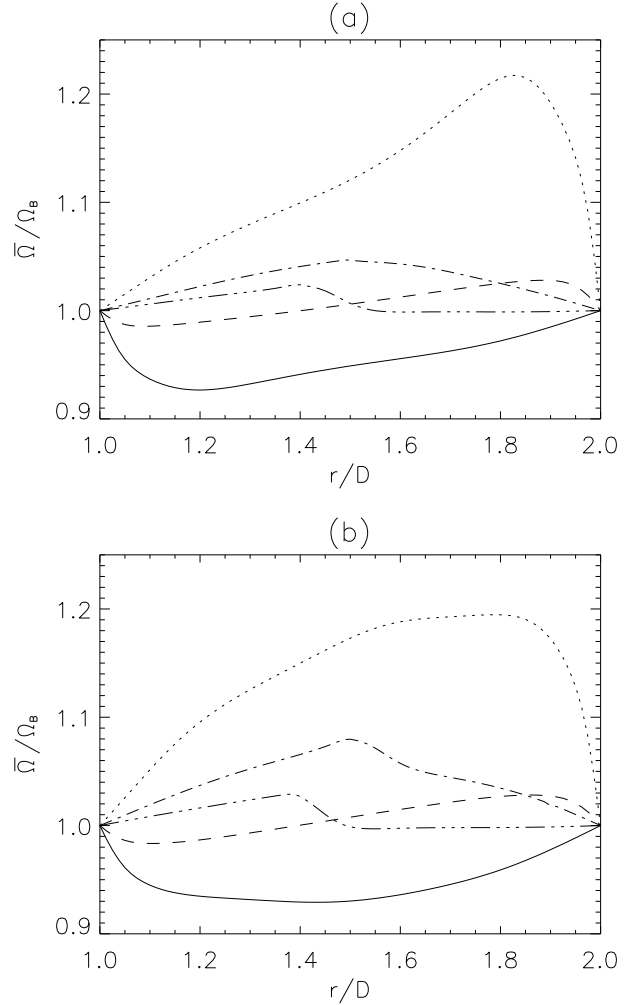


Fig. 5 Deviations of the averaged $\bar{\Omega}(r)$ from the basic state $\Omega_0(r)$ for different vertical boundary conditions; rigidly rotating endplates (both with Ω_{end}): — $\Omega_{\text{end}} = \Omega_{\text{out}}$, \cdots $\Omega_{\text{end}} = \Omega_{\text{in}}$, --- $\Omega_{\text{end}} = \Omega_{\text{endmin}}$; divided into two rings: $\dashv\dashv$ $w_1 = 0.5$, $\cdots\dashv$ $w_1 = 0.4$. (a) $\text{Re} = 1000$, $\text{Ha} = 0$, (b) $\text{Re} = 1000$, $\text{Ha} = 10$.

background. We clearly see the instability and structure of traveling vortices, the frequency of this motion agrees with the predictions based on the linear analysis (see e.g. Rüdiger et al. 2005).

As we have shown above, one can obtain a much better basic state for the finite cylinders by dividing endplates into two rings. The results for such conditions are presented in Fig. 6b. We notice that the background state quickly becomes entirely steady. Naturally the Ekman pumping mechanism is still present in this case, and traces of two Ekman vortices can be seen. The flow, however, is laminar. For $\beta = 6$ the pattern of the traveling vortices is clearly more regular (cf. Fig. 6b, right).

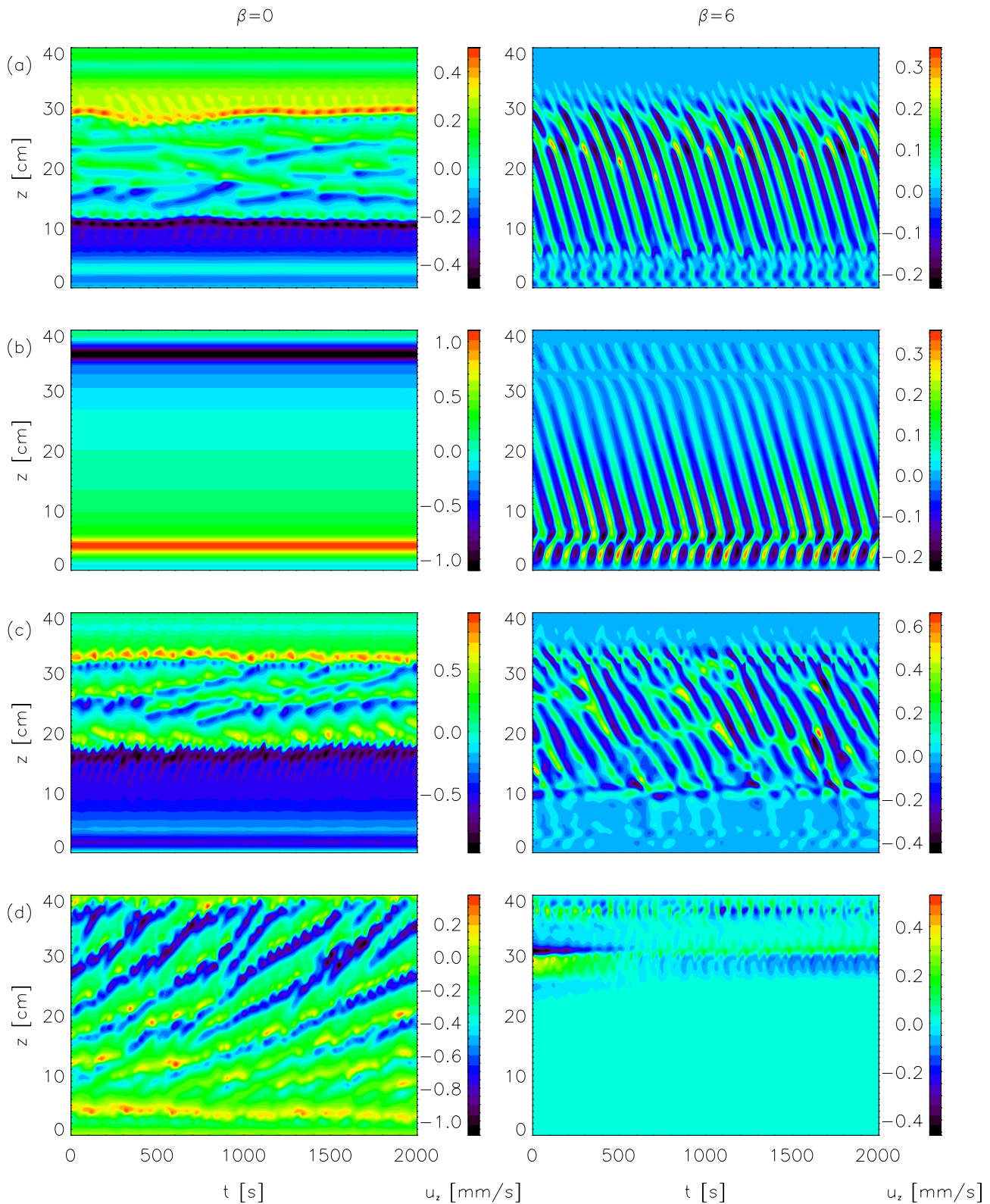


Fig. 6 The axial velocity $u_z(z, t)$ at $r = R_{\text{in}} + 0.6D$ as a function of time t and z . *Left*: basic state $\beta = 0$. *Right*: $\beta = 6$, the averaged $u_z(t)$ is subtracted in order to eliminate the background from the velocity field, except in (d). (a): both endplates rotate rigidly with $\Omega_{\text{end}} = \Omega_{\text{out}}$. (b): both endplates are divided into rings attached to the cylinders; the inner ring has the width $0.4D$. (c), (d): the bottom endplate is stationary $\Omega_{\text{bot}} = 0$, the upper rotates with $\Omega_{\text{top}} = \Omega_{\text{out}}$. (a), (b), (c): insulating endplates, $\text{Re} = 1775$ ($\Omega_{\text{in}} = 0.377$ Hz), $\text{Ha} = 9.5$. (d): perfectly conducting endplates, $\text{Re} = 1000$, $\text{Ha} = 10$. The traveling wave frequency for (a), (b), (c) is respectively $f/\Omega_{\text{in}} = 0.0294$, 0.0253 , 0.0292 whereas the linear stability analysis yields $f/\Omega_{\text{in}} = 0.0258$.

When one considers two endplates with different rotational properties, additional velocity and current gradients in the vertical direction arise and disturb further the flow. It is clearly seen in Fig. 6c that disturbances exist in the case where the upper endplate rotates with $\Omega_{\text{top}} = \Omega_{\text{out}}$, and the bottom one is fixed, $\Omega_{\text{bot}} = 0$. The background flow for $\beta = 0$ is highly irregular and time-dependent, especially in the middle part of the cylinder, the circulation close to the endplates is roughly steady. Nonetheless, the external B_ϕ produces, again, a clear periodic motion with a frequency corresponding to that of the helical MRI.

Using conducting boundaries instead of insulating ones leads to an increase of the Ekman circulation and the Hartmann current, the latter being drawn from the plates. This current is significantly stronger than the current generated in the Ekman-Hartmann layer, and therefore we expect that an experiment with conducting plates would undergo additional problems due to magnetic forces acting on the fluid. Let us consider a perfectly conducting endplates with asymmetric rotation (again at the top $\Omega_{\text{top}} = \Omega_{\text{out}}$ and at the bottom $\Omega_{\text{bot}} = 0$), then there exists an important gradient in the radial current which, acting in concert with the axial magnetic field, is strong enough to “drag” vortices in the direction of decreasing field strength. This situation is shown in Fig. 6d where we see a periodic vertical motion even if $\beta = 0$. Moreover, if we introduce a toroidal field with appropriate sign (i.e. positive in this case) it will act against the force due to the current gradient and can reduce the periodic vertical motions in the flow (Fig. 6d, right panel). If B_ϕ would have a different sign both effects would interact resulting in a highly irregular time-dependent behavior.

We notice that in the real PROMISE experiment the bottom endplate rotating with Ω_{out} (which, after taking into account the directions of rotation and the applied magnetic field, corresponds to the top endplate in our simulations) was made of copper, and the stationary top endplate (bottom in the simulations) was made of plexiglass. Therefore an additional asymmetry in the magnetic boundary conditions was present. Although copper is a good conductor it should not be directly compared with perfectly conducting boundaries used in the simulations since the latter represent stronger assumptions and induce stronger currents. However it is clear that using insulating material on both ends would prevent additional currents from disturbing the flow.

3.3 Critical values

Noting that the background state for sufficiently fast rotation and rigidly rotating endplates $\Omega_{\text{end}} = \Omega_{\text{out}}$ is not steady, it is interesting to investigate what happens when a spiral magnetic field with strength below the critical value is applied. One could expect that a viscous process (like the Ekman pumping) excites fluctuations which could then be amplified and, due to geometry of the applied magnetic field, drifting.

Figure 7 shows that for endplates causing strong disturbances the traveling wave can indeed be observed even

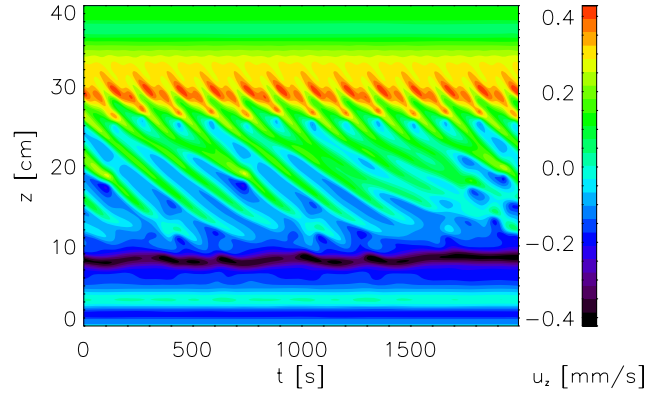


Fig. 7 Profiles of $u_z(z, t)$ for $\text{Re} = 1775$, $\text{Ha} = 9.5$, $\beta = 2$ and rigidly rotating ends with $\Omega_{\text{end}} = \Omega_{\text{out}}$. The critical β_c for the corresponding Re , Ha in the limit of infinite cylinders is $\beta_c = 2.56$, and one would expect that the traveling wave decays. This is not the case for the boundary conditions shown here where a clear periodic motion is visible. Its frequency $f/\Omega_{\text{in}} = 0.0124$ agrees with the prediction of a linear analysis for marginal stability in the limit of infinite cylinders, yielding $f/\Omega_{\text{in}} = 0.0120$. However, the latter approach yields negative growth rate (exact numbers for frequencies and wavenumbers for the linear results presented in this paper were provided by R.Hollerbach who used them to generate figures in Rüdiger et al. (2006).

for subcritical characteristic values. This is also somewhat in agreement with the experiment – traces of moving vortices were observed for states which are stable in the limit of infinite cylinders. We see that the amplitudes of the vertical component of the velocity u_z are almost unchanged when compared to the background state (Fig. 6a, left). Although the pattern of the vortices is not very regular, there exists a clear frequency peak for the vertical traveling wave. The frequency and the drift direction (which is reversed by a sign change of, for example, β) corresponds to results of the linear analysis for infinite cylinders. This leads to the conclusion that, although excitations do not grow due to helical MRI, still the same mechanism is responsible for the drift.

If two rings are used and the basic state is steady the situation changes since the additional excitations due to the endplates are minimized. Surprisingly, it is possible that even for supercritical parameters the traveling wave, although excited for a moment, decays (see Fig. 8). It is still possible to get sustained instability by increasing, for example, β (see Fig. 6b).

The reason for this damping might be height of the cylinders which does not match an integer value of the vertical wavenumber k . For $\text{Re} = 1775$, $\beta = 5$, $\text{Ha} = 9.5$ the corresponding wavelength is $\lambda = 2\pi D/2.1728$ and does not suit the assumed aspect ratio $\Gamma = H/D = 10$. If the height was changed to $\Gamma = 4\lambda = 11.57$ the observed decay of the traveling wave was significantly slower, so slow that after the sudden switching on of the external azimuthal magnetic field the wave could be observed with the PROMISE facility still several hours later. Bearing in mind that wave-

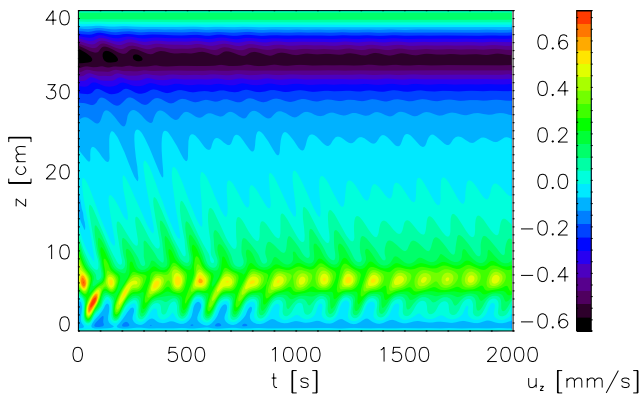


Fig. 8 The velocity $u_z(z, t)$ for $Re = 1775$, $Ha = 9.5$, $\beta = 5$ and endplates divided into two rings with $w_1 = 0.4$. Although in the limit of infinite cylinders the flow is unstable, we clearly see that the disturbances (which developed after a sudden switch on of the magnetic field) decay. The frequency of the decaying wave is $f/\Omega_{in} = 0.0237$ which again is in agreement with f from the result of the linear analysis, $f/\Omega_{in} = 0.0232$.

lengths for given Reynolds numbers are longer with decreasing beta (for $\beta = 3$, $k = 1.45D^{-1}$, $\beta = 1$, $k = 0.6D^{-1}$), the constant height of the cylinders ($\Gamma = 10$ in the experiment) can be an issue when looking for critical numbers. It should be noted that due to the boundary layers the effective region where the traveling wave can exist for configuration with two rings is smaller than Γ by approximately $0.5D$ (distances up to about $0.25D$ from the endplates are influenced by their presence).

Although endplates clearly can serve as the source of viscous excitations and the axially traveling wave develops also for subcritical parameters, we shall notice that there are no periodic motions in the background state. In this sense the “imperfect” background state serves as a catalyst for the helical MRI instability. When the endplates are divided into rings the resulting hydrodynamic flow is laminar, and only after the magnetic field is applied the periodic fluctuations occur, and, moreover, their frequency corresponds exactly to that predicted from the linear analysis for infinite cylinders.

Liu et al. (2006) suggested that the observed fluctuations can have their origin in the underlying hydrodynamical unsteady flow as reported, for example, by Kageyama et al. (2004). In the latter work the purely hydrodynamic flow for $Re \approx 1000$ with rigidly rotating ends $\Omega_{end} = \Omega_{out}$ and short aspect ratio $\Gamma = 1$ was already unsteady. We confirm these results with the method used here. However if longer cylinders are used, like $\Gamma = 10$, the flow becomes steady for $Re = 1000$, and only after imposing strong enough magnetic fields (say $Ha = 12$, $\beta = 6$) a traveling wave develops with a frequency that matches calculations from the linear analysis.

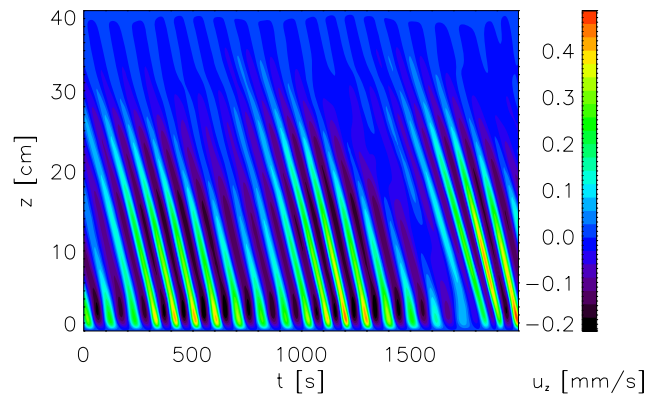


Fig. 9 The velocity $u_z(z, t)$ for $Re = 1775$, $Ha = 9.5$, $\beta = 6$ and endplates rotating differentially so that $\Omega_{end} = \Omega_0$.

3.4 Differentially rotating ends

We have also performed simulations for differentially rotating plates with ideal Couette profile for periodic cylinders so that $\Omega_{end}(r) = \Omega_0(r)$. In another recent work (Liu, Goodman & Ji 2007) it has been shown that for parameters corresponding to $Re = 1775$, $Ha \approx 10$, $\beta \approx 4$ the traveling wave decays for such boundary conditions. We confirm this result with our method, although our treatment of the magnetic boundaries is simplified.

The explanation for this fact might be again the inappropriate height of the cylinders which is far from an integer value of the expected vertical wavelength. For these parameters $\lambda = 3.476D$ according to the linear theory so that less than three wavelengths can fit in the container. On the other hand, if $\beta = 6$ is used, $\lambda = 2.49D$ and then $\Gamma = 10$ almost exactly corresponds to 4λ . From Fig. 9 we see indeed that in this case persistent fluctuations exist with a frequency corresponding to the helical MRI instability. We have also made calculations for $\beta = 4$ with longer cylinders so that $H = 4\lambda D = 13.90D$ and $\Gamma = 5\lambda D = 17.38D$. In each case a sustained traveling wave has been observed. It should be mentioned that the vortices do not develop very close to the upper boundary so that it is convenient to take longer cylinders.

4 Summary

It is easier to perform an experiment showing spiral MRI because a much slower rotation of the cylinders is required for the instability to set in compared with MRI with an axial magnetic field only. Moreover, there exists additional quantity, i.e. drift frequency, which is easy to measure and can serve as an important indicator for the associated phenomena. It is claimed that in the PROMISE experiment frequencies and amplitudes corresponding to the spiral MRI were observed, and the results agreed with theoretical calculations of both linear and nonlinear 2D simulations (see Stefani 2007) for a review). However it is still possible to improve the experiment so that the basic state is a completely steady flow.

In this paper we have presented a relatively simple and inexpensive modification which is suitable for such an improvement. Firstly, the endplates should be both made of insulating material and both should rotate in the same way so that the system is symmetric in the z direction. Secondly, it is convenient to divide the lids into two rings which can be attached to the cylinders so that no separate driving is needed. The optimal, width of the inner ring, in the sense of minimizing the induced azimuthal magnetic field, is 1.6 cm for the current experimental setup.

Our calculations also show that spiral MRI modes can be driven by endplate effects even for subcritical characteristic values (see Fig. 7). On the other side when providing a steady background flow by applying rings one has to pay more attention to the height of the cylinders and to take into account the vertical wavelengths of the traveling wave which depend on the magnetic configuration. For the current aspect ratio $\Gamma = 10$ and $Re = 1775$ it is reasonable to consider $Ha = 9.5$, $\beta = 6$ which almost exactly corresponds to $\Gamma = 4\lambda$.

References

- Abshagen, J., Cliffe, K. A., Langenberg, J., Mullin, T., Pfister, G., Tavener, S.J.: 2004, *ThCFD* 18, 129
- Balbus, S.A., Hawley, J.F.: 1991, *ApJ* 376, 214
- Barenghi, C.F., Youd, A.J., Willis, A.P.: 2004, in: R. Rosner, G. Rüdiger, A. Bonanno (eds.), *MHD Couette Flows: Experiments and Models*, AIPC 733, p. 83
- Burin, M.J., Ji, H., Schartman, E., Cutler, R., Heitzenroeder, P., Liu, W., Morris, L., Raftopolous, S.: 2006, *ExFl* 40, 962
- Ekman, V.: 1905, *Ark. Mat. Astr. Fys* 2, 1
- Hollerbach, R., Fournier, A.: 2004, in: R. Rosner, G. Rüdiger, A. Bonanno (eds.), *MHD Couette Flows: Experiments and Models*, AIPC 733, p. 114
- Hollerbach, R., Rüdiger, G.: 2005, *PhRvL* 95, 124501
- Ji, H., Goodman, J., Kageyama, A.: 2001, *MNRAS* 325, L1
- Ji, H., Goodman, J., Kageyama, A., Burin, M., Schartman, E., Liu, W.: 2004, in: R. Rosner, G. Rüdiger, A. Bonanno (eds.), *MHD Couette Flows: Experiments and Models*, AIPC 733, p. 21
- Ji, H., Burin, M., Schartman, E., Goodman, J.: 2006, *Nature* 444, 343
- Kageyama, A., Ji, H., Goodman, J., Chen, F., Shoshan, E.: 2004, *physics/0405123*
- Liu, W., Goodman, J., Ji, H.: 2007, *astro-ph/0703525*
- Liu, W., Goodman, J., Herron, I., Ji, H.: 2006, *PhRvE* 74, 056302
- Noguchi, K., Pariev, V.I., Colgate, S.A., Beckley, H.F., Nordhaus, J.: 2002, *ApJ* 575, 1151
- Roberts, P. H.: 1967, *An Introduction to Magnetohydrodynamics*, Longmans, Green and Co. Ltd.
- Rüdiger, G., Zhang, Y.: 2001, *A&A* 378, 302
- Rüdiger, G., Schultz, M., Shalybkov, D.A.: 2003, *PhRvE* 67, 046312
- Rüdiger, G., Hollerbach, R., Schultz, M., Shalybkov, D.A.: 2005, *AN* 326, 409
- Rüdiger, G., Hollerbach, R., Stefani, F., Gundrum, T., Gerbeth, G., Rosner, R.: 2006, *ApJL*, 649, L145
- Stefani, F., Gundrum, T., Gerbeth, G., Rüdiger, G., Schultz, M., Szklarski, J., Hollerbach, R.: 2006, *PhRvL* 97, 184502
- Stefani, F., Gundrum, T., Gerbeth, G., Rüdiger, G., Szklarski, J., Hollerbach, R.: 2007, *astro-ph/0701030*
- Szklarski, J., Rüdiger, G.: 2006, *AN* 327, 844
- Velikhov, E.P.: 1959, *SJETP* 36, 995
- Wendt, G.: 1933, *AnP* 409, 445
- Youd, A.J., Barenghi, C.F.: 2006, *JFM* 550, 27
- Zikanov, O., Thess, A.: 1998, *JFM* 358, 299